PCCP

Accepted Manuscript

This is an *Accepted Manuscript*, which has been through the Royal Society of Chemistry peer review process and has been accepted for publication.

Accepted Manuscripts are published online shortly after acceptance, before technical editing, formatting and proof reading. Using this free service, authors can make their results available to the community, in citable form, before we publish the edited article. We will replace this *Accepted Manuscript* with the edited and formatted *Advance Article* as soon as it is available.

You can find more information about *Accepted Manuscripts* in the **Information for Authors**.

ROYAL SOCIETY OF CHEMISTRY

www.rsc.org/pccp

PCCP

Pressure-induced penetration of guest molecules in high-silica zeolites: the case of mordenite

R. Arletti[a], L. Leardini[b], G. Vezzalini[c], S. Quartieri[b], L. Gigli[a], M. Santoro[d,e], J. Haines[f]., J. Rouquette[f], L. Konczewicz[g]

A synthetic high-silica mordenite (HS-MOR) has been compressed in both non-penetrating (silicone oil, s.o.) and penetrating [methanol:ethanol:water (16:3:1) (m.e.w.), water:ethanol (3:1) (w.e.), ethylene glycol (e.gl.)] pressure transmitting media (PTM). In situ, high-pressure (HP) synchrotron X-ray powder diffraction (XRPD) experiments allowed the unit cell parameters to be followed up to 1.6, 1.8, 8.4, and 6.7 GPa in s.o., w.e., m.e.w., and e.gl., respectively. Moreover, e.gl. was also used as a PTM in in situ HP Raman and ex situ IR experiments. The structure refinement of HS-MOR compressed in e.gl. at 0.1 GPa - the lowest investigated pressure - revealed the presence of 3.5 ethylene glycol molecules per unit cell. The infrared spectrum of the recovered sample, after compression to 1 GPa, is consistent with the insertion of ethylene glycol molecules in the pores. XRPD and Raman spectra under pressure indicated the insertion of a small number of guest molecules. Ethylene glycol is partially retained inside mordenite upon pressure release. A symmetry lowering was observed in s.o. above 0.8 GPa, while above 1.6 GPa the patterns indicated a rapid loss of long range order. From ambient pressure (P_{amb}) to 1.6 GPa, a high cell volume contraction (ΔV=-9.5%) was determined. The patterns collected with penetrating PTM suggested the penetration of guest molecules into the host porous matrix, starting from a very low P regime. The entrapping of PTM molecules inside micro porosities contributes to stiffen the structure and, as a consequence, to decrease the compressibility with respect to that measured in s.o. From the structural point of view, HS-MOR reacts to compression and to the penetration of the different guest species with proper framework deformations. Interestingly, ethylene glycol is partially retained inside mordenite upon pressure release, which is interesting for potential applications of this composite material.

Introduction

Zeolites have been found to maintain their crystallinity at high pressure (HP) without major structural modifications[1] and with only moderate changes of pore shape, even when a volume contraction as high as 15% is observed.[2] In experimental HP studies of zeolites, either 'pore penetrating' or 'non-penetrating' pressure-transmitting media (PTM) are used. The former are usually aqueous/alcohol mixtures, with molecular sizes small enough to penetrate zeolite pores (see ref. 3 for a review); the latter are

usually silicone oil or glycerol with molecules too large to penetrate (see e.g. ref. 4, 5, 6, 7, 8, 9, 10, 11, 12, 13).

High-pressure studies performed using pore penetrating media have attracted great attention for the so called Pressure-Induced Hydration effect (PIH)[14], in which the water content inside the cavity increases in response to the applied pressure through selective sorption of H_2O molecules from the PTM.

Several experimental and theoretical studies have been performed to investigate water intrusion mechanisms in all-silica zeolites (ref. 15 and references therein). Understanding the properties of water systems confined within hydrophobic surfaces is relevant in applications where all-silica zeolites or activated carbons are used (e.g. inhibition of corrosion, design of super-hydrophobic surfaces[16,17]). The spontaneous condensation of water in the nanopores of a hydrophobic silicalite (framework type MFI)[18] and of an all-silica ferrierite (framework type FER)[19] was recently investigated with a combined mercury porosimetry and Gran Canonical Montecarlo simulation study. Water intrusion/extrusion has been investigated by theoretical methods in many hydrophobic microporous frameworks (e.g. AFI, IFR, MTW, TON, CHA, see e.g. 20). In some cases, zeosils behave like water springs, since water intrusion is reversible upon pressure release, (e.g. MFI, FER, BEA, CHA) (see e.g. ref. 21), in other cases, hysteresis is observed during the extrusion stage (RUB-41, ITQ-7)[22] and zeosils behave as shock

[a] Dipartimento di Scienze della Terra, Università di Torino, Via Valperga Caluso 35, I-10125 Torino, Italy
[b] Dipartimento di Fisica e Scienze della Terra, Università di Messina, Viale Ferdinando Stagno d'Alcontres 31, I-98166 Messina S. Agata, Italy
[c] Dipartimento di Scienze Chimiche e Geologiche, Università di Modena e Reggio Emilia, Via Campi 103, I-41125 Modena, Italy
[d] Istituto Nazionale di Ottica, INO-CNR, via N. Carrara 1, I-50019 Sesto Fiorentino, Italy
[e] European Laboratory for Non Linear Spectroscopy (LENS), Via N. Carrara 1, I-50019 Sesto Fiorentino, Italy.
[f] Institut Charles Gerhardt Montpellier, UMR 5253 CNRS, Equipe C2M, Université de Montpellier, Place E. Bataillon, cc1504, 34095 Montpellier, Cedex 5, France
[g] Laboratoire Charles Coulomb, UMR 5221 CNRS, Université de Montpellier, Place E. Bataillon, 34095 Montpellier, Cedex 5, France.

Electronic Supplementary Information (ESI) available: [atomic coordinates, bond distances, X-ray diffraction patterns]. See DOI: 10.1039/x0xx00000x

absorbers. An irreversible behavior, with water molecules trapped in the micropores upon pressure release, is reported for ITQ-4, which behaves as a bumper.[23]

Rather few studies are available in literature on the HP-intrusion and self-organization of organic molecules in zeolite pores. Among these, the possibility of HP-induced polymerization has recently been demonstrated for acetylene and ethylene inserted into the MFI framework.[24,25] Pressure is the most efficient means to reduce intermolecular distances, thereby allowing chemical reactions to occur.[25] The studies performed with 'non-penetrating' media highlighted the crucial influence of the framework type and composition, and of the extra-framework content, on a zeolite's response to pressure in terms of deformation mechanism and compressibility.[2,5,10,11,12] Zeolite compressibility does not appear directly related to material porosity, while it is more closely related to the characteristics of the extra-framework cations, and the number of H_2O molecules. As a consequence, some zeolites characterized by large pores can be unexpectedly less compressible than other pure-Si phases with empty cavities. Various authors [7, 8, 9 10, 11,12,13] came to the same conclusions working on materials sharing the same framework type, but with different extra-framework and framework compositions.

The compression of zeolites using non-penetrating media has also been exploited to induce the so-called "pressure-induced amorphization" (PIA). [26, 27, 28, 29, 30, 31, 32, 33, 34 35.36, 37, 38] PIA is observed for a wide range of silicate structures and is accompanied by significant volume reductions, resulting in a new denser material. For some zeolites, PIA is irreversible in the presence of small extra-framework cations (e.g. H) and reversible when larger ones or water are hosted in the pores (e.g. Li and Na).

This paper reports the HP behavior of a high-silica mordenite (HS-MOR). Understanding the stability of mordenite under non-ambient conditions is of great interest because of the role of this porous material in many industrial processes. In fact, mordenite is increasingly used as molecular sieve for the adsorptive separation of gas or liquid mixtures involving acidic components, and is also used extensively as a catalyst for several important reactions like hydrocracking, hydroisomerization, alkylation, reforming, and cracking.[39, 40] In its Si-rich form, mordenite has been used for the adsorption of pollutants from aqueous media.[41, 42, 43, 44, 45, 46] Otherwise, it is worth noting that mordenite has never been exploited up to now to incorporate organic molecules upon pressure.

In this work we have compressed HS-MOR in both penetrating and non-penetrating PTM with the following aims:

i) to verify the possibility of HP-induced water intrusion in this hydrophobic high-silica zeolite and hence to interpret the mechanisms of possible selective adsorption (for example in water purification) when all-silica zeolites are used;
ii) to test the degree of reversibility of the water intrusion process: the onset of a reversible/irreversible cycle makes the material suitable for applications such as springs, shock absorbers, or bumpers;
iii) to verify the possible penetration of different organic molecules and determine the pressure value necessary to achieve this effect;
iv) to study the HP-induced structural deformations and the possible occurrence of PIA phenomena;

v) to verify the possible self-assembling of the intruded molecules and/or to understand the host/guest interactions after intrusion.

Mordenite: structure and previous non ambient studies

Mordenite (framework type MOR[47], space group *Cmcm a* = 18.0519(8), *b*= 20.2061(8), *c* = 7.4506(3), V = 2717.7(2)) is both a well-known zeolite mineral[48,49] and a synthetic porous material [50]. Its crystal structure[51] (Figure 1) is built up from an assembly of single 6-membered ring (6MR) sheets linked by single 4MR or else from a combination of 5-1 secondary building units. MOR exhibits a 1D channel system comprising three different channel types: i) large 12MR channels (''free diameters'' 6.5x7.0 Å) parallel to the *c* axis; ii) strongly elliptic 8MR channels (''free diameters'' 2.6x5.7 Å) also parallel to the *c* axis; iii) sinusoidal channels with limiting 8MR windows (''free diameters'' 3.4 x 4.8 Å) parallel to the *b* axis. The 8MR and 12MR channels running along the *c* axis are interconnected along the [010] direction through side pockets delimited by double 8MRs, which are part of the wall of the sinusoidal channel. Mordenite has an orthorhombic unit cell of topological space-group symmetry *Cmcm*. The real symmetry of the mineral is reduced to *Cmc*2_1[50] (thus avoiding a straight T–O–T angle), but the crystal structure remains strongly pseudo-centro-symmetric.
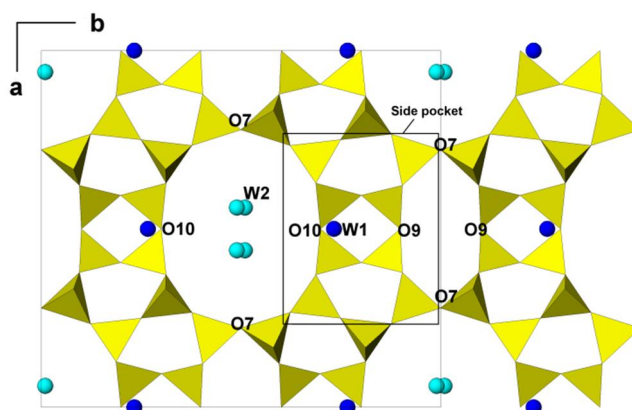

Figure 1. MOR framework structure viewed along the [001] direction. The side pocket, delimited by the 8-membered rings of the sinusoidal channel, is marked in the figure. W1 and W2 water molecules are colored in blue and light blue, respectively. The unit-cell is indicated by the solid line.

Mordenite has been studied at high temperature (HT) by several authors by means of thermogravimetric analysis, and in situ and ex situ HT X-ray diffraction.[52] The high pressure (HP) behavior of a synthetic Na-mordenite $Na_6Al_{6.02}Si_{42.02}O_{96}\cdot 19H_2O$ was investigated by Gatta and Lee[53] by in situ synchrotron XRPD up to 5.68 GPa, using m.e.w. as PTM. No phase transition was observed within the pressure range investigated. Strong anisotropic elastic behavior along the *a*, *b,* and *c* axes (with the compressibility of b>c>a) was reported. The reasons for the observed anisotropic compression were intuitively assumed on the basis of the ambient pressure crystal structure of mordenite and of the HT structural

behavior. In the paper, the authors suggest that the structure reacts to pressure by increasing the ellipticity of the channel systems, since any ''inversion'' in ellipticity would be energetically unfavorable. The evolution of the unit-cell parameters gave no evidence of PIH. However, the lack of structural refinements prevented unambiguous descriptions of the P-induced effects at the atomic level.[54] A further HP study performed on the same Na–mordenite sample by in situ single-crystal synchrotron XRD, using 4:1 methanol:ethanol mixture as PTM, showed a phase transition from a C-centered to a primitive space group: possibly *Pbnm*, *Pbnn* or *Pbn*2_1 - probably displacive in character - between 1.68(7) and 2.70(8) GPa.[55] The structural refinements enabled description of the deformation mechanisms in the low-P regime: bulk compression is greatly accommodated by increasing the ellipticity of the large 12-membered ring channels running along [001]. The authors suggest that the higher compressibility observed for the sample in methanol and ethanol, compared to that observed in m.e.w., might be due to the latter sample undergoing a P-induced over-hydration effect.

The sample used in this work is a commercial high-silica mordenite (HS-MOR hereafter, SiO_2/Al_2O_3 ratio ~ 200; Na_2O < 0.1 wt.%) purchased from the Tosoh Corporation (Japan) in its protonated form (code HSZ-690HOA). This material was characterized by different techniques (SEM, surface area and porosimetric analysis, thermogravimetric analysis, and FTIR spectroscopy) and was used in previous work on the adsorption of pollutants from waste water.[41,42,43,44,45,46] FTIR spectroscopy revealed the presence of a large quantity of silanol defects produced by the dealumination process.[44] The high concentration of silanols explains the ability of this sample to adsorb the significant amount of water determined by TG analysis, which should be stabilized in the side pockets where the majority of defects are located.

Experimental
Thermogravimetric analysis

Thermogravimetric analysis (TGA) was carried out using a Seiko SSC 5200 thermal analyzer in order to determine the water content. The sample was loaded in a Pt crucible and heated in an air flux (100 µL min-1) from room temperature up to 850 °C (increment rate 10 °C min-1).

XRPD experiment at ambient conditions

A preliminary synchrotron XRPD at ambient conditions of the HS-MOR sample was performed at the SNBL1 (BM01a) beamline at ESRF (Grenoble). The diffraction data (λ = 0.69736 Å) were collected in the Debye–Scherrer geometry on a MAR345 image plate (IP) detector. The powder was placed in a 0.3 mm quartz capillary mounted on a goniometric spinning head. A one-dimensional diffraction pattern was obtained by integrating the two dimensional image with the program FIT2D [56]. Rietveld profile fitting was performed in the Cmcm space group using the GSAS package [57] with the EXPGUI [58] interface, starting from the framework atomic coordinates reported in 41. The extraframework water molecules were localized from the difference Fourier map. The background curve was fitted using a Chebyshev polynomial with 18 coefficients. The pseudo-Voigt profile function proposed by 59 was applied and the peak intensity cut-off was set to 0.1% of the peak maximum. The 2θ-zero shift, scale factor, and unit-cell parameters were accurately refined. Soft-restraints were applied to the T–O distances (1.60 Å) and the weight was gradually decreased, after the initial stages of refinement, up to a final weight of 100. The isotropic displacement parameters were constrained in the following way: the same value for all tetrahedral cations, a second value for all framework oxygen atoms, and a third value for water oxygen atoms. Details of the structural refinements are reported in Table 1. Atomic coordinates, occupancy factors, and thermal parameters along with bond distances (Å) within the mordenite framework are reported as Supplementary Material (Tables 1S and 2S, respectively). The dimensions of the channel apertures along with their ellipticity (E, the ratio between the largest and the smallest O-O diameters) and their Crystallographic Free Area (CFA) *sensu*[47] are reported in Table 2, while the final observed and calculated HS-MOR powder patterns at $\underline{P}_{amb}$ are provided in Figure 1SA in Supplementary Material

Table 1. Details of the structural refinements parameters.

	P_{amb}	Silicone Oil		Ethylene Glycol	
		0.2 GPa	0.8 GPa	0.1 GPa	P_{amb} (rev)
Space group	*Cmcm*	*Cmcm*	*Cmcm*	*Cmcm*	*Cmcm*
a (Å)	18.0519(8)	18.0005(14)	17.8703(20)	18.082(2)	18.091(1)
b (Å)	20.2061(8)	20.1118(13)	19.7888(17)	20.259(2)	20.287(1)
c (Å)	7.4506(3)	7.4249(4)	7.3460(6)	7.4703(5)	7.4701(4)
V (Å^3)	2717.7(2)	2687.98(31)	2597.8(4)	2736.6(4)	2741.6(3)
R_{wp} (%)	3.56	9.05	10.27	9.62	9.7
R_p (%)	2.56	7.01	8.32	7.62	7.7
R_F^2 (%)	6.03	11.55	15.61	9.36	9.97
N_o of contributing reflections	1659	1661	1656	2106	1597
N_{obs}	607	564	537	752	754
N_{var}	61	61	61	70	70

Table 2. Dimensions of the channel apertures within the HS-MOR framework in ambient conditions (P_{amb}(cap), in capillary), compressed in s.o. at 0.2 and 0.8 GPa and compressed in e.gl. at 0.1 GPa and upon pressure release (P_{amb} (rev)).

	Silicone oil			Ethylene Glycol	
	P_{amb} (cap)	0.2 GPa	0.8 GPa	0.1 GPa	P_{amb} (rev)
12MR					
O7-O7	10.02(3)	10.08(2)	10.08(3)	10.05(2)	10.01(3)
O10-O10	8.85(5)	8.80(3)	8.33(3)	8.92(3)	8.94(3)
E*	1.13	1.15	1.21	1.12	1.12
CFA** (Å^2)	35.10	35.62	33.43	36.08	36.03
8MR					
O7-O7	8.03(3)	7.92(2)	7.79(3)	8.05(2)	8.08(3)
O9-O9	5.58(4)	5.45(2)	5.27(3)	5.50(2)	5.51(3)
E	1.44	1.45	1.48	1.46	1.47
CFA (Å^2)	10.61	10.22	9.78	13.03	13.16

In situ high-pressure XRPD experiments

In situ high-pressure synchrotron XRPD experiments were performed at the SNBL1 (BM01a) beamline at ESRF (Grenoble), using different pressure media: silicone oil (s.o.) as non-penetrating PTM; (16:3:1) methanol:ethanol:water (m.e.w.), (3:1) water:ethanol (w.e.), and ethylene glycol (e.gl.) as penetrating ones. The diffraction data were collected using modified Merril-Basset DACs [60] with fixed wavelengths of 0.69736 Å for the experiments performed in s.o., w.e. and m.e.w., and 0.68253 Å for the experiment performed in e.gl. Pressure was measured using the ruby fluorescence method[61] with the non-linear hydrostatic pressure scale.[62] The estimated error in the pressure values is 0.05 GPa.[62] MAR345 and Pilatus IP detectors (with pixel dimensions 150 and 172 µm, respectively) were used at fixed distance of 230 mm for the experiments performed in s.o., w.e. and m.e.w. and 193 mm for that in e.gl., respectively. The exposure times were 300 s for all the pressure points. The powder patterns were collected in the following *P* ranges: P_{amb}-8 GPa, 0.3-2.0 GPa, 0.1-11.8 GPa, and P_{amb}-8.8 GPa, for the experiments performed in s.o., w.e., m.e.w., and e.gl., respectively. In the case of w.e., the limited *P* range investigated was due to the formation of ice VII at about 2 GPa.

A Raman study performed by Murly et al.[63] on pure ethylene glycol under pressure evidenced a liquid-solid transition at about 4 GPa, suggested by the appearance of external Raman modes and observed visually. However, for a comparison with the other HP experiments, the results of HS-MOR compressed in e.gl. are reported for the complete P-range.

Some patterns (labeled (rev) in Tables and Figures) were measured while decompressing the samples down to ambient conditions, in order to test the reversibility of the P-induced effects.

One-dimensional diffraction patterns were obtained by integrating the two dimensional images with the FIT 2D program. [56] The refinement of cell parameters was carried out by means of the Rietveld method using the GSAS package[57] with the EXPGUI interface[58] starting from the structural model obtained at ambient conditions and adopting the same refinement strategies described in section 3.2. Up to the highest investigated P, the original orthorhombic *Cmcm* space group was used in the unit-cell refinements. The unit-cell parameters were refined up to 1.6, 1.8, 8.4, and 6.7 GPa in s.o., w.e., m.e.w., and e.gl., respectively (Table 3).

The quality of the powder patterns collected in s.o. at 0.2 and 0.8 GPa and in e.gl. at P_{amb} and upon pressure release allowed

complete structural refinements to be performed. The refinement strategy was the same as that employed for the experiment at ambient conditions. In the s.o. refinements, due to the limited quality of the data, soft constraints were applied not only to the T-O distances (1.60 Å) but also to the O-O distances (2.60 Å) and the weight was gradually released up to a final value of 2000. Figure 1S (B-E) reports the final observed and calculated powder patterns for s.o. at 0.2, and 0.8 GPa., and for e.gl. at 0.1 GPa and P_{amb} (rev). Atomic coordinates, occupancy factors, and thermal parameters are provided in Table 1S and 2S of the Supplementary Material. Table 2 reports the dimensions of the channel apertures, their ellipticity parameters (E defined as the ratio between the largest and the smallest O-O diameters), and their Crystallographic Free Area (CFA) *sensu*[47] as a function of P.

In situ high-pressure Raman experiments

Raman measurements on mixtures of HS-MOR powder and ethylene glycol as a PTM compressed from 0.1 to 9.2 GPa were performed by using the 647.1 nm line of a Kr⁺ laser as the excitation source. The backscattering geometry was used through a 20× Mitutoyo micro-objective, NA=0.28, and the unpolarized signal was detected by a single monochromator (Acton/SpectraPro 2500i) equipped with different diffraction gratings and a CCD detector (Princeton Instruments Spec-10:100BR). Spectral resolutions varied from 0.6 to 6 cm⁻¹. Transverse and longitudinal spatial resolutions were equal to 2.5 µm and 15 µm, respectively.

Piston cylinder experiment and ex situ powder diffraction

A mixture of HS-MOR powder and ethylene glycol as a pressure medium were placed in the UNIPRESS piston cylinder device. The diameter and height of the sample volume were 6 mm and 70 mm, respectively. The pressure was gradually increased up to 1 GPa and then held for 3 hours followed by decompression. The pressure was measured with a manganin gauge.

Table 3. Unit-cell parameters of HS-MOR as a function of P, obtained using s.o., w.e., m.e.w., and e.gl. as pressure transmitting media.

P (GPa)	a (Å)	b (Å)	c (Å)	V (Å^3)
		s.o.		
0.2	18.001(1)	20.112(1)	7.4249(4)	2688.0(3)
0.8	17.870(2)	19.789(2)	7.3460(6)	2597.8(4)
		Pbnm		
1.2	17.749(2)	19.610(1)	7.2931(5)	2538.4(3)
1.6	17.556(2)	19.388(2)	7.2261(7)	2459.6(4)
		Pbn2$_1$		
1.2	17.749(2)	19.610(1)	7.2931(5)	2538.4(3)
1.6	17.559(2)	19.390(2)	7.2260(7)	2460.2(4)
		w.e.		
0.3	18.059(2)	20.234(2)	7.4571(6)	2724.9(5)
0.6	18.058(3)	20.200(3)	7.4456(8)	2715.9(6)
0.8	18.056(3)	20.181(3)	7.4384(8)	2710.4(7)
0.9	18.052(3)	20.172(3)	7.4342(9)	2707.1(7)
1.1	18.039(4)	20.162(3)	7.428(1)	2701.6(8)
1.3	18.019(4)	20.164(3)	7.424(1)	2697.4(8)
1.6	17.972(4)	20.191(4)	7.421(1)	2693(1)
1.7	17.955(5)	20.206(4)	7.421(1)	2692(1)
1.8	17.938(5)	20.222(4)	7.421(1)	2692(1)
P$_{amb}$ (rev)	18.059(3)	20.253(2)	7.4568(8)	2727.3(6)
		m.e.w.		
0.1	18.048(1)	20.213(1)	7.4494(4)	2717.6(3)
0.2	18.048(2)	20.204(2)	7.4471(5)	2715.6(4)
0.3	18.046(2)	20.186(2)	7.4416(5)	2710.9(4)
0.6	18.046(2)	20.164(2)	7.4331(5)	2704.8(4)
0.9	18.042(2)	20.147(2)	7.4230(7)	2698.1(5)
1.2	18.034(2)	20.131(2)	7.4133(8)	2691.4(5)
1.7	18.002(3)	20.123(2)	7.3998(9)	2680.5(6)
2.1	17.963(3)	20.132(3)	7.3909(9)	2672.8(6)
2.8	17.900(3)	20.106(3)	7.370(1)	2652.3(7)
3.7	17.808(4)	19.969(3)	7.328(1)	2605.9(8)
4.6	17.716(4)	19.809(4)	7.283(1)	2555.8(9)
5.2	17.654(5)	19.705(4)	7.252(2)	2523(1)
5.5	17.625(5)	19.652(5)	7.238(2)	2507(1)
6.5	17.526(6)	19.498(6)	7.193(2)	2458(1)
7.1	17.478(7)	19.419(6)	7.169(2)	2433(1)
7.8	17.416(7)	19.319(7)	7.140(2)	2402(2)
8.4	17.367(8)	19.236(7)	7.117(2)	2377(2)
4.0 (rev)	17.796(5)	19.943(4)	7.316(2)	2596(1)
1.6 (rev)	18.002(3)	20.146(3)	7.3996(9)	2683.6(6)
P$_{amb}$ (rev)	18.061(2)	20.262(2)	7.4516(5)	2726.9(4)
		eth.g.		
0.1	18.082(2)	20.259(2)	7.4703(5)	2736.6(4)
0.2	18.080(2)	20.250(2)	7.4673(6)	2733.9(4)
0.4	18.078(2)	20.230(2)	7.4624(6)	2729.2(4)
0.5	18.073(2)	20.203(2)	7.4553(7)	2722.1(5)
0.8	18.065(2)	20.172(2)	7.4468(7)	2713.6(5)
1.0	18.042(2)	20.125(2)	7.4324(7)	2698.6(5)
1.3	18.018(2)	20.097(2)	7.4222(7)	2687.6(5)
1.7	17.977(2)	20.063(2)	7.4088(7)	2672.1(5)
1.9	17.942(2)	20.035(2)	7.3977(7)	2659.2(5)
2.3	17.901(2)	19.992(2)	7.3828(7)	2642.1(5)
2.8	17.843(2)	19.899(2)	7.3564(8)	2611.9(5)
3.4	17.786(3)	19.804(3)	7.3304(9)	2582.0(6)
4.0	17.722(3)	19.684(2)	7.2985(9)	2546.0(6)
4.4	17.680(3)	19.609(2)	7.2784(8)	2523.3(5)
5.0	17.639(3)	19.529(2)	7.2558(9)	2499.5(5)
5.7	17.618(3)	19.477(3)	7.239(1)	2484.0(6)
6.1	17.601(3)	19.444(5)	7.229(1)	2474.1(6)
6.7	17.585(3)	19.409(3)	7.218(1)	2463.4(7)
3.0 (rev)	17.843(3)	19.902(2)	7.3494(8)	2609.8(6)
P$_{amb}$ (rev)	18.091(1)	20.287(1)	7.4701(4)	2741.6(3)
P$_{amb}$ (rev)				
ex situ	18.072(5)	20.253(3)	7.462(1)	2731(1)

The powder recovered from the compression was measured on a Laboratory Siemens D5000 diffractometer equipped with a CuKα radiation (1.54056 Å) on a zero background sampleholder from 2 to 120° 2θ with an angular step of 0.02° and counting time of 10 secs per step. The XRPD pattern is reported in supplementary materials (Figure 2S).

Ex-situ IR experiments

Infrared spectra on the initial HS-MOR and on the sample recovered at ambient pressure (P_{amb}) after compression at 1 GPa in piston cylinder (see previous section) were collected using a Horiba Jobin-Yvon Labram Aramis spectrometer equipped with an Olympus microscope and an attenuated total reflection (ATR) objective.

Results

Thermogravimetric analysis (TGA)

Thermogravimetric analysis (Figure 2) shows an overall weight loss of about 8 %. Taking into account the weight loss attributed to the removal of weakly bonded physisorbed water molecules (about 4 %), the structural water content corresponds to about 6 molecules per unit cell. In the 425-850 °C range, the DTA curve shows a broad endothermic event due to the condensation of the silanol groups.
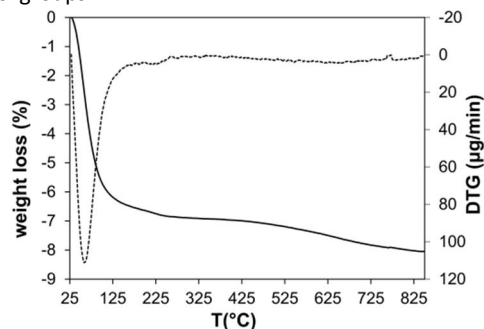

Figure 2. TG (solid line) and DTG (dotted line) of the HS-MOR sample.

Structural refinement of HS-MOR at ambient conditions

The results of the structural refinement of HS-MOR at ambient conditions are in close agreement with those given by Martucci et al.[41] Four tetrahedral rings can be identified in the mordenite framework: the 12MR and 8MR delimiting the straight channels (Figure 1), and the 8MRs delimiting the *inlet/entry* and the *outlet/exit* of the sinusoidal channel (referred to as 8MR-A and 8MR-B, respectively). All these rings exhibit an elliptical shape as indicated by their E values reported in Table 2.

Two partially occupied extraframework sites were localized from the difference Fourier map and attributed to water molecules: W1, located in the side pocket, and W2 residing in the 12MR channel (Figure 1). The presence of water molecules in the side pocket is not accidental since the silanol defects are mainly located in this structural unit.[45] As a whole, 3.6 water molecules/u.c. (corresponding to about 2.2 wt %) were found. The remaining 2.4 molecules necessary to fit the TG results are probably disordered and distributed over a number of crystallographic sites. W1-O5 bond distance (3.17(2) Å) suggests weak interactions between this molecule and the framework. In contrast, no interactions between W2 and the framework oxygen atoms were observed

HS-MOR compressed in silicone oil: results of the structure refinement

Figure 3 shows selected integrated powder patterns of HS-MOR compressed in s.o. The peak intensities decrease and the peak profiles become broader with increasing pressure, in particular above 1.6 GPa. However, complete X-ray amorphization is not achieved up to the highest investigated pressure, even though the P-induced deformations are not reversible upon decompression (Figure 3A). Above 0.8 GPa, the appearance of three weak reflections not allowed by the *Cmcm* symmetry (Figure 3B) suggests a symmetry lowering. A similar result has recently been reported by Lotti and coworkers for a Na-mordenite, compressed in

methanol:ethanol 4:1 between 1.68(7) and 2.70(8) GPa [55]. The authors suggest a lowering from *Cmcm* to *Pbnm* or *Pbnn* s.g. (or from *Cmc*2$_1$ to *Pbn*2$_1$ when starting from the acentric *Cmc*2$_1$ s.g.). In the present case, the best fit was obtained assuming the *Pbnm* and *Pbn*2$_1$ s.g.. The refinement of the cell parameters - determined by the Le Bail method – using both space groups at 1.2 and 1.6 GPa gave the same values (Table 3). Hence, *Pbnm* and *Pbn*2$_1$ s.g. could be considered possible space groups. Above this pressure, the rapid deterioration in quality of the diffraction data prevented any data analysis.
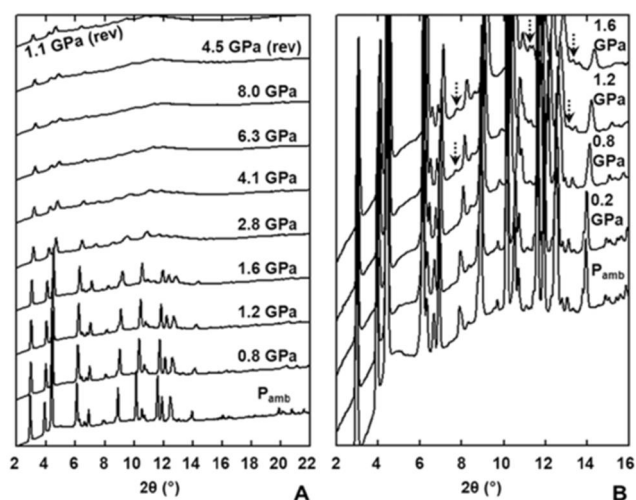
Figure 3 (A) Selected integrated powder patterns of HS-MOR compressed in s.o.. (B) 2θ range from 2 to 16° of the lowest P powder patterns. The arrows point to the new peaks indicating the phase transition.

Normalized unit-cell parameters are shown in Figure 4. All unit-cell parameters decrease as a function of P, with a higher compression along the *b* axis. The corresponding unit-cell volume contraction up to 1.6 GPa is Δ*V* = -9.5%. Above 0.8 GPa, in parallel with the symmetry change, a slope change in the unit-cell parameter evolution is visible, corresponding to an increase in compressibility**.**

Rietveld refinements of the powder patterns collected at 0.2 and 0.8 GPa indicated that the 12MRs and 8MRs windows of the channels running along the *c* axis become more compressed along their original shorter O-O diameters, as revealed by the ellipticity values reported in Table 2. This increase in ellipticity is accompanied by a narrowing of these apertures, as suggested by their CFA values (Table 2). At the same time, a shrinkage is also observed in the 8MRs of the sinusoidal channel, without any change in their ellipticity.
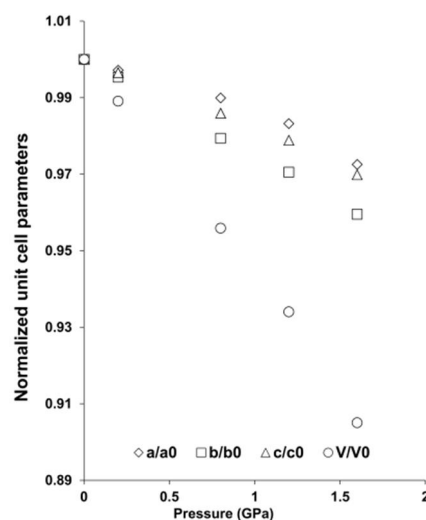

Figure 4. Normalized unit-cell parameters and volume of HS-MOR compressed in s.o.

HS-MOR compressed in penetrating media

Figure 5 reports the powder patterns collected at the lowest investigated pressure with the different penetrating PTM, compared to that of HS-MOR at ambient pressure in capillary. A first analysis reveals significant differences in the peak intensity ratios. In particular, a decrease in the intensity of the low 2θ angle diffraction peaks − strongly dependent on the amount and distribution of the extraframework species − is observed for all the media. This suggests the penetration of medium molecules even in the very low *P* regime.
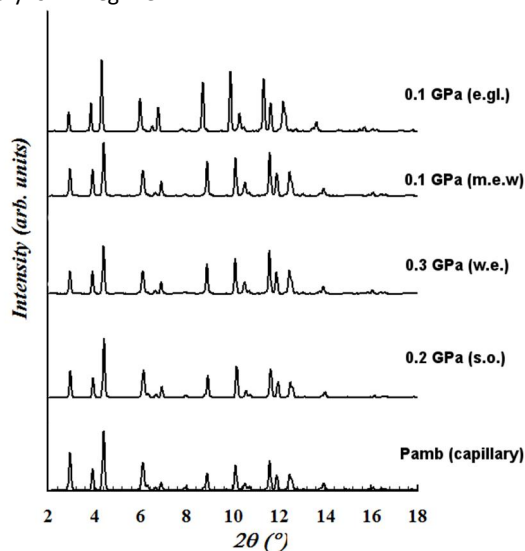

Figure 5. Comparison among the powder pattern of the HS-MOR sample in capillary (P$_{amb}$) and those of the sample loaded in DAC with the different PTM at the lowest investigated pressure.
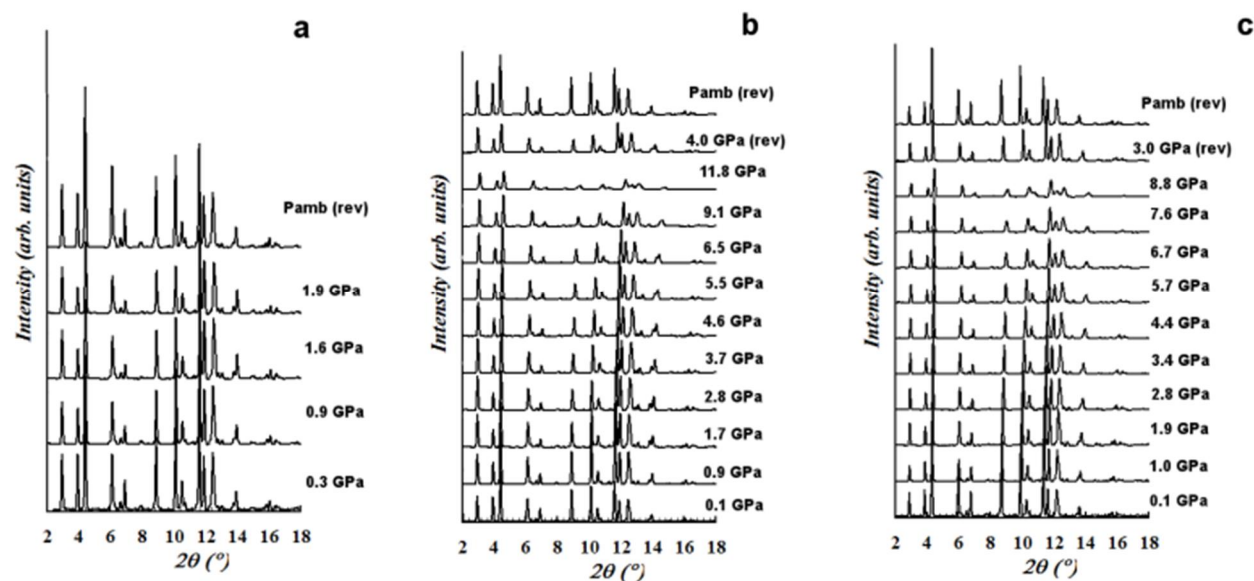
Figure 6. Selected integrated powder patterns of HS-MOR compressed with penetrating PTM. (a) w.e. (b) m.e.w. (c) e.gl.
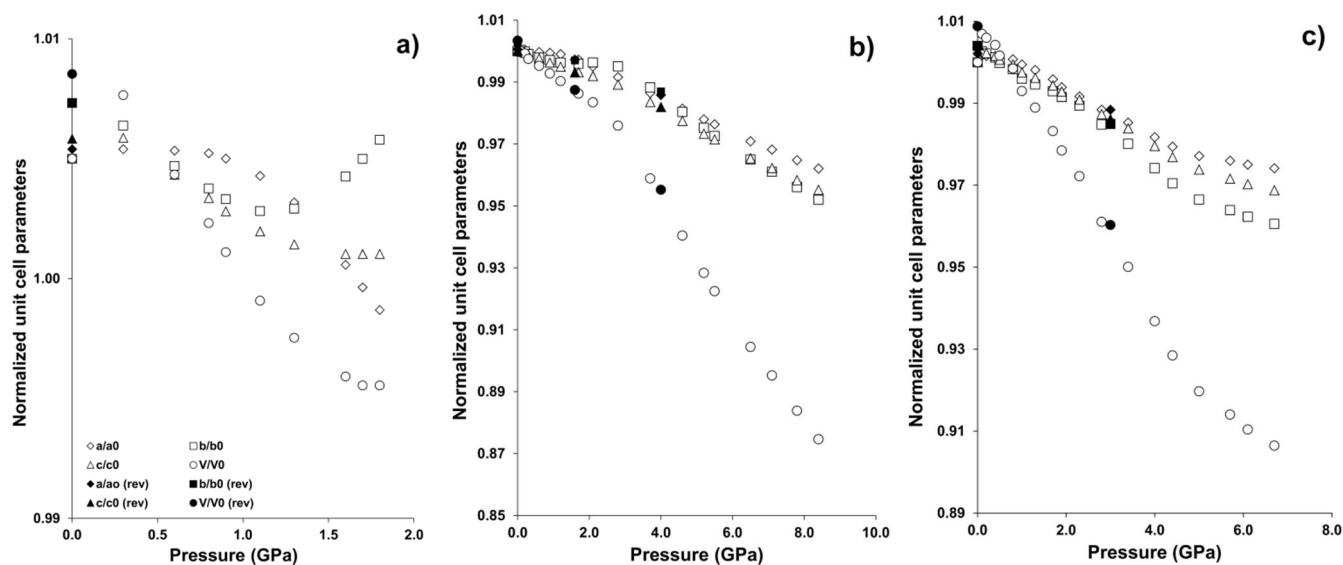

Figure 7. Normalized unit-cell parameters of HS-MOR compressed in (a) w.e., (b) m.e.w and (c) e.gl. as a function of P.

An inspection of Figure 6, showing sequences of selected integrated powder diffraction patterns of HS-MOR compressed with the various penetrating media, leads to the following general results, in summary form:

i) a gradual and slight broadening of the peak profile is observed with increasing P, without complete amorphization within the investigated P range;

ii) no phase transitions or symmetry lowering are observed in the studied P ranges;

iii) a change in the peak intensity ratios (especially at low 2θ angle) is already observed at very low P values;

iv) the P-induced effects are partially reversible upon decompression. An almost complete recovery of the initial diffraction peak positions is observed for all the systems, with the only exception of HS-MOR compressed in m.e.w., in which a shift towards lower 2θ values of the peaks is evident (Table 3). In contrast, the original intensity ratios were not completely regained upon decompression to P_{amb} in any of the experiments. This effect is particularly evident in the e.gl. experiment.

Figure 7 shows the evolution of the normalized unit-cell parameters of HS-MOR as a function of P for the different PTM. The overall cell-axes and cell-volume variations are the following:

- e.w. (ΔP= 0.3-1.8 GPa): Δa=-0.63%, Δb=0.07%, Δc=-0.40%, ΔV=-0.94%.
- m.e.w. (ΔP= 0.1-8.4 GPa): Δa=-3.79%, Δb=-4.80%, Δc=-4.48%, ΔV=-12.54%.
- e.gl. (ΔP = P_{amb}-6.7 GPa): Δa=-2.59%, Δb=-3.94%, Δc=-3.12%, ΔV=-9.36%.

HS-MOR compressed in ethylene glycol: results of the structure refinement

The structure refinement of HS-MOR compressed in e.gl. was possible only for the data collected at 0.1 GPa - the lowest investigated pressure- and at P_{amb} (rev). The details of the refinements are reported in Table 1, while the atomic coordinates of the two structures are presented in the Supplementary Information (Tables 1S and 2S). On the basis of the Fourier difference map, at 0.1 GPa it was possible to locate 3.5 ethylene glycol molecules per unit cell, distributed in two different configurations, both in the 12MR channel (Figure 8).

One configuration (e.gl.1) is characterized by the C-C bond aligned along the [001] direction, with the C atoms lying on the mirror plane ⊥ to [100] and the two hydroxyls in two crystallographically equivalent positions (OH1 in Table 1S and 2S and in Figure 8).
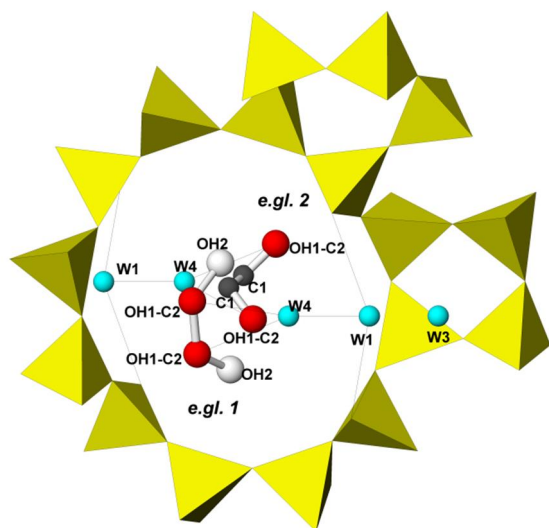

Figure 8. Projection along [001] of the HS-MOR structure compressed in e.gl. at 0.1 GPa. The two e.gl. configurations (1 and 2) are shown. OH1 and C2 sites are crystallographically equivalent

The second configuration (e.gl.2) has the C-C bond aligned along the [100] direction, with the two hydroxyls (OH2) equivalent for the mirror m ⊥ to [100]. Both these configurations can be described as gauche conformers, following 63. The refined occupancy factors give 1.9 and 1.6 e.gl.1 and e.gl.2 molecules p.u.c., respectively. This corresponds to the presence of 0.95 e.gl.1 and 0.8 e.gl.2 in each 12MR channel p.u.c. at 0.1 GPa. It is worth noting that, on the basis of the steric hindrance, every 12 MR channel can host only one molecule in e.gl.1 and one molecule in e.gl.2 configuration, or two molecules in e.gl.2 configuration. The

structural refinements hence indicate that, even at the lowest investigated pressure, the channel is almost completely filled. This is consistent with the structural variations undergone by the zeolite framework: a widening of the 12MR – accompanied by an increasing of the ellipticity of the 8MR (Table 2) – and an increase of 0.7% of the cell volume (Table 1) at 0.1 GPa, necessary to accommodate the intruded molecules.

Along with the organic molecules, 4.4 water molecules were located in the Fourier difference map over three independent crystallographic sites, all lying on the mirror plane perpendicular to [100]: W1 (already present in the P_{amb} structure), W3, located in the side pocket, and W4 in the 12MR ring. Part of the water molecules occupying the site W2 in the structure at ambient conditions were probably relocated in the W4 site after the ethylene glycol intrusion, since the original W2 is very close to e.gl.2 molecule. The number of water molecules found at 0.1 GPa (4.4(3)) is slightly higher than that found at P_{amb} conditions (3.6(3) per u.c.). This new value, which is in better agreement with the results of TG analysis (6 water molecules p.u.c.), could be the consequence of a more ordered distribution of the water molecules over the extraframework sites, favored by the imposed pressure.

The interactions among the framework and the ethylene glycol molecules are water-mediated: both e.gl.1 and e.gl.2 molecules are at bond distance from W4, which, in turn interacts with W1, which coordinates 2 oxygen atoms in the side pocket. When simultaneously present in the channel, the two ethylene glycol molecules can interact each other via a weak hydrogen bond (OH1-OH2: 2.70 Å).[63]

Notwithstanding the high pressure reached during the in-situ experiment (P max 8.8 GPa), the features of the pattern collected in DAC upon decompression to P_{amb} are similar to those found at 0.1 GPa upon compression. The framework - which definitely underwent strong deformations at HP revealed by a cell volume variation at 6.6 GPa of -9.4 % - regains a structure similar to that of low pressure (see Table 1S, 2S with the e.gl. molecules in the same positions observed at 0.1 GPa (Figure 9).
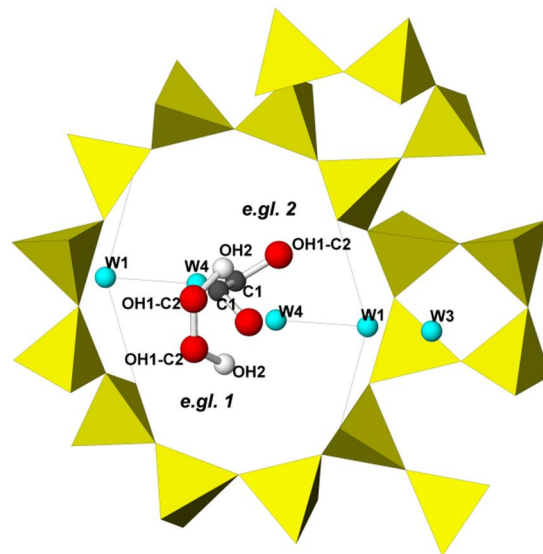

Figure 9. Projection along [001] of the HS-MOR structure in e.gl. at P_{amb} after pressure release. The two e.gl. configurations (1 and 2) are shown. OH1 and C2 sites are crystallographically equivalent

The difference between the two refinements concerns, on the contrary, the occupancy factors calculated for the two e.gl. configurations. Of the overall 3.4 molecules p.u.c found in the channels, 2.6. are in the e.gl.2 configuration (*vs*. 0.8 molecules p.u.c. at 0.1 GPa). This could originate from the pursuit of a better packing of the molecules in the channels at high pressure. In fact, as previously discussed, two e.gl.2 (but only one e.gl.1) can be hosted in each channel.

Seven water molecules were found in the structure upon decompression. As previously discussed, this could derive from a further ordering induced by high pressure on the originally disordered water distribution.

On the basis of the data collected at P_{amb}(rev), we could conclude that the e.gl. intrusion is irreversible. Actually, the phenomenon could be partially reversible considering that, due to the lack of data on the high pressure structures, we cannot exclude the penetration of further additional e.gl. molecules, then extruded during decompression.

The XRPD pattern collected in laboratory on the powder recovered from the ex-situ HP experiment in piston cylinder did not allow structural refinements to be performed. Nevertheless, the refined cell parameters show that the cell volume of the recovered form is larger than that of the original HS-MOR (Tables 1 and 3). This can be a further indication of the permanent insertion of some e.gl. molecules in the porosities and that a pressure of about 1 GPa is sufficient to induce an - at least partially - irreversible e.gl. molecular intrusion.

HS-MOR compressed with ethylene glycol: IR and Raman results

The IR spectrum of HS-MOR sample is principally characterized by a very strong Si-O stretching mode near 1061 cm^{-1} and weaker peaks near 1230, 952 and 820 cm^{-1} (Figure 10). Weak peaks at 3360 and 1628 cm^{-1} due to hydrogen bonded vicinal silanol groups [45] and/or H_2O molecules are also present. A series of additional peaks at for example 2942, 2879, 1652, 1458, 1413, 1370, 1339, 882 and 862 cm^{-1} are observed in the spectrum of the recovered sample corresponding with very high precision (typically ± 1 cm^{-1}) to the spectrum of ethylene glycol (http://webbook.nist.gov). The main OH stretching peak (3325 cm^{-1}) is shifted to lower wavenumbers with respect to the ethylene glycol reference (3375 cm^{-1}), which is indicative of stronger hydrogen bonding. Another evident change is the appearance of a new peak in the Si-O stretching region at 1027 cm^{-1}, which is the strongest peak in the spectrum. Peaks are expected for e.gl. at 1085 and 1040 cm^{-1}, but their intensities are lower than this new peak. The initial Si-O peak only shifts slightly from 1061 to 1064 cm^{-1}.

The presence of this new strong peak is an indication of an important interaction between the extraframework species (water and inserted e.gl. molecules) and the SiO_2 framework of HS-MOR. Such a shift to lower wavenumber could be also an indication of a reduction in certain Si-O-Si angles linked to changes in diameter and ellipticity of the 12MR and 8MR observed by XRPD due to pore filling by ethylene glycol.

In Figure 11 we report selected Raman spectra measured on a mixture of HS-MOR powder and ethylene glycol upon pressure increase between 0.1 GPa and 9.2 GPa.
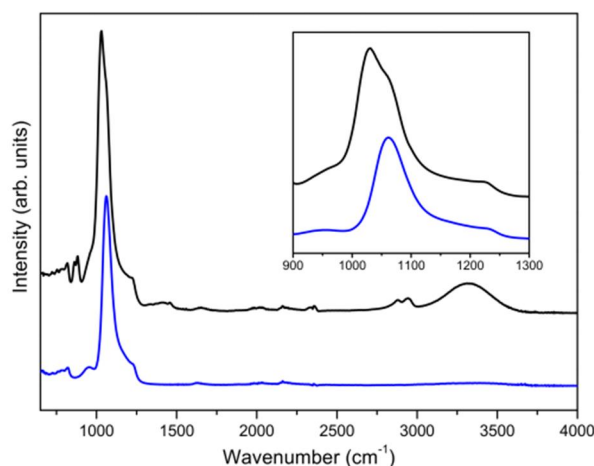

Figure 10. Attenuated total reflection (ATR) infrared spectra of pure HS-MOR powder (bottom-blue) and a mixture of HS-MOR powder and e.gl., (top-black) measured after compression to 1 GPa. The splitting of the main Si-O stretching band is shown in the inset. The other additional peaks in the spectrum of the mixture are due to e.gl. (see text).

The aim of this measurement was to identify potential peaks of e.gl. confined in HS-MOR. At each pressure we show a spectrum measured in a point where only pure bulk e.gl. was present, and a one where HS-MOR and e.gl. occupied two roughly equal portions of the scattering volume. In this last case the spectra are dominated by the strong molecular peaks of e.gl., whereas the very weak peaks of HS-MOR are barely visible at about 400-470 cm^{-1}, partially overlapped by those of e.gl. Moreover, the peaks of e.gl. around HS-MOR and in the pure bulk almost coincide, which indicates these peaks being entirely due to bulk e.gl. and, as a consequence, no signatures of confined e.gl. are detected.
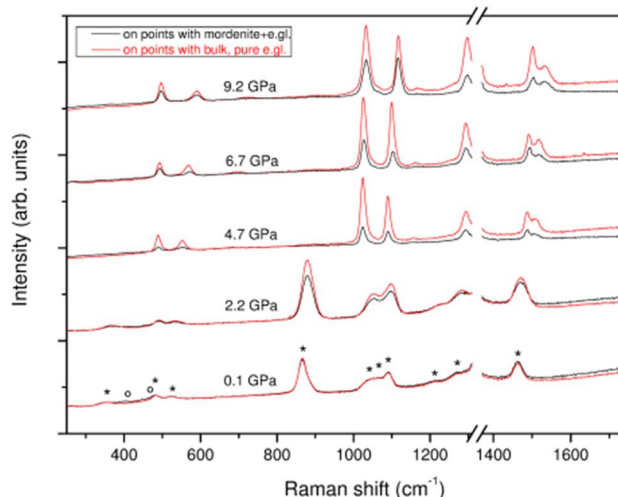

Figure 11. Raman spectra of a mixture of HS-MOR powder and e.gl., measured upon pressure increase. Red lines: pure bulk e.gl.; black line: HS-MOR+e.gl.. Stars: peaks of e.gl.; circles: peaks of HS-MOR. Spectral resolution: 6 cm^{-1}. The same peaks were observed with a spectral resolution of 0.6 cm^{-1}. Crystallization occurs above about 4 GPa. The spectra have been normalized to the same intensity at 600-650 cm^{-1}, and then vertically shifted for the sake of clarity.

Pressure evolution of the spectra, along with the visual observation, show bulk crystallization of e.gl. above 4 GPa. For the symmetry assignment of the Raman spectrum and for pressure induced phase transitions of e.gl. we refer to ref. 63 and references therein. The lack of Raman signatures of confined e.gl. does not disagree with our XRPD analysis, which indicates that the amount of confined e.gl. molecules –and hence of potential Raman scatterers of this type in the HS-MOR unit-cell– is as low as 3.5 at 0.1 GPa. As a reference, we can consider the case of simple molecules such as CO_2 and C_2H_2 confined at 0.5-26 GPa in silicalite, a pure SiO_2 zeolite whose primitive cell accommodates up several tens of these small extra-framework molecules.[64,65,66] In these studies we have been showing Raman peaks of the confined molecules, which are shifted by 10-15 cm^{-1} at several GPa with respect to those of the bulk molecular material, due to the confinement effects and the interaction with the walls of the host zeolite. In addition, the peaks of the confined medium were weaker than those of the bulk part by even one order of magnitude, when the zeolite and the pure, surrounding molecular material occupied almost equal portions of the scattering volume. In the present case of HS-MOR and e.gl., since we have about one order of magnitude less confined guest molecules, we expect the Raman peaks of these ones being weaker than those of their bulk counterpart by even two orders of magnitude, which would make the peaks hard to detect.

Discussion

Structural deformations induced by non-penetrating PTM

The HP-induced modifications of HS-MOR unit-cell parameters are strictly related to the variations in the geometry and dimensions of the 12MRs and 8MRs channels. The larger and shorter diameters of the two straight 12MRs and 8MRs channels running along [001] are aligned along the *a* and *b* axes, respectively (Figure 1 and Table 2). The higher compressibility observed in s.o. along the *b*-axis (*b>c>a*), is consistent with the results of the structural refinements performed up to 0.8 GPa (i.e. before the phase transition). These data indicate an increase in ellipticity of these rings, due to the shortening of their shorter diameters aligned along the *b*-axis (Table 2). A strong anisotropic elastic behavior of *a*, *b,* and *c* axes (with *b>c>a*) was also reported for Na-MOR compressed in m.e.w.[54], whose anisotropic compression was interpreted on the basis of the MOR HT-structural behavior [52]. It was argued that under hydrostatic compression the structure reacts by increasing the original ellipticity of the channels.

Above 0.8 GPa, HS-MOR compressed in s.o. undergoes a phase transition which has also been reported for Na-MOR by ref.54. Phase transitions even in a low *P* regime is not uncommon, in fact have also been reported for the high-silica zeolites silicalite-1 [9,15,67] and Si-FER.[68] These studies demonstrate that high-silica zeolites, when compressed in non-penetrating PTM, undergo marked framework deformations as a consequence of the lack of the extraframework species, which cannot contribute to stiffen the structure. Thus it is not surprising that these zeolites accommodate H*P* induced distortions by changing their symmetry.

After the phase transition, the *b*-axis is still the most compressible, thus it is reasonable to assume a further increase in

the ellipticity of the 12MR and 8MR channels. Since a rapid loss of long range order and a strong peaks broadening is observed above 1.6 GPa, it is possible that, at higher P, this process could reach a geometrical limit and hence favor material "amorphization". A significant peak broadening is also reported in literature for a purely siliceous faujasite compressed in s.o. above 2.2 GPa[69] and was interpreted as the onset of amorphization. Haines et al.[70] also reported a very strong decrease in intensity just above 3 GPa in a calcined hydrophobic silicalite-1-F, with complete disappearance of the diffraction lines just above 8.6 GPa. In the present case, although no complete X-ray amorphization is achieved up to the highest investigated P, the P-induced effects are only partly irreversible upon decompression. The relatively low stability of the studied mordenite could also be influenced by the presence of a large amount of structural silanol defects, as revealed by IR spectroscopy studies[44,45] and confirmed in the IR spectrum of the HS-MOR sample reported in this study.

Structural deformations induced by penetrating PTM

The structural response of HS-MOR compressed in penetrating PTM is different from that observed when compressed in s.o.. The occurrence of a phase transition at very low pressure in s.o. ramp and the availability of only few high pressure volume data did not allow the calculation of B0 values. Anyway, to have a clear idea of the compressibility on the different systems, it is possible to compare the ΔV in the same pressure range (P_{amb}-0.8 GPa). The compressibility observed in e.gl. ($\Delta V P_{amb}$-0.8GPa=0.15)., m.e.w. ($\Delta V P_{amb}$-0.9GPa=0.72) and e.w. ($\Delta V P_{amb}$-0.8GPa=0.41) is lower than in s.o. ($\Delta V P_{amb}$-0.8GPa=4.41). Aqueous/alcohol mixtures (w.e. and m.e.w.) and ethylene glycol have molecular sizes compatible with the dimensions of the channel apertures and, in principle, could all penetrate mordenite micro-porosities. The trend observed for the three penetrating PTM is slightly different. In fact, for HS-MOR in e.gl., at the first investigated pressure (0.1 GPa) a strong volume increase (ΔV=0.7%) is observed. Even if all the cell parameters undergo a lengthening, the most marked increase is along the *b* axis*.* This could be the consequence of the penetration of the ethylene glycol molecules in the 12MR channel, whose shorter diameter (O10 – O10 in Table 2) needs an expansion to facilitate the intrusion of the molecules. This, along with the structural data obtained from the pattern collected at 0.1GPa – showing the presence of 3.5 e.gl molecules per unit cell – indicates a rapid intrusion of the molecules in HS-MOR structure in the very first stage of the compression. The lack of structural data at higher pressures prevented us from knowing whether in the subsequent compression steps the HS-MOR channels would reach the maximum occupancy for e.gl. molecules (estimated in 4 molecules per unit cell considering the crystallographic positions found at 0.1 GPa).

Above 0.1 GPa, the unit cell volume of HS-MOR in e.gl. starts to decrease, as a consequence of the compression of all the cell parameters, following the trend already observed for s.o. experiment (b>c>a). A change in the slope of the volume curve, indicating a change of the elastic behavior and an increase in the compressibility, is observed at 1.7 GPa, when, probably, the molecules end their penetration in the channels. In fact, in the low

P regime – when the pores are almost empty and the main process underway is the P-induced pore intrusion – the applied pressure acts mainly by pushing molecules into the zeolite material and only by partly compressing it. After insertion of the guest species (here at 1.7 GPa), the applied pressure acts predominantly by compressing and distorting the zeolite framework, thereby giving rise to the increased compressibility evident in Figure 12.

As previously reported, both XRD and IR data provide evidence for the penetration of e.gl. in the HS-MOR porosities upon compression. Due to the lack of structural information on the aqueous/alcohols systems, the behavior of HS-MOR compressed in
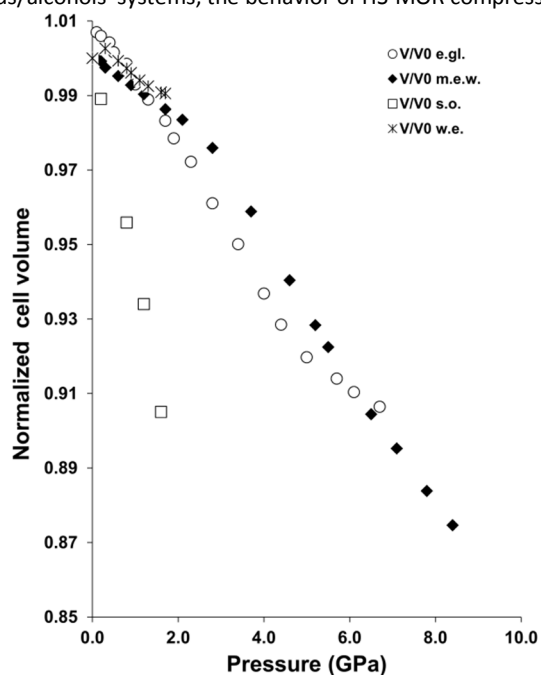

Figure 12. Comparison of the normalized cell volume variation as a function of P for HS-MOR compressed with non-penetrating (s.o.) and penetrating (w.e.; m.e.w.; e.gl.) PTM.

w.e. and in m.e.w. can be interpreted only on the basis of the changes of the cell parameters and of the relative intensity of the diffraction peaks. The changes in the intensity ratios of the low-2θ diffraction peaks observed at very low pressure (Figure 5), suggest an immediate and continuous penetration of additional guest species into the channels. The P-induced intrusion of guest molecules is also confirmed by comparing the volume contraction of HS-MOR compressed in s.o. and in penetrating PTM in the P_{amb}-1.2 GPa range (Figure 12). The lower compressibility observed with penetrating media can be ascribed to the intrusion of additional guest molecules, which contribute to stiffen the mordenite framework.

HS-MOR compressed in aqueous media does not show the marked cell volume increase observed in e.gl.. In w.e. the volume increase is only 0.25%, while in m.e.w. the cell volume remains almost constant during the first compression step. This is probably due to the molecular dimensions of water and alcohols, which are smaller than ethylene glycol, thus demanding a less marked framework deformation. The limited volume increase, in w.e. is accompanied by an increase of 0.3% of b parameter from 1.3

GPa to the highest investigated pressure. This behavior, which is not observed in m.e.w. could be due to the penetration of different amount/type of guest molecules.

As for the compression in e.gl., an increase of HS-MOR compressibility (due to the end of the molecular intrusion process) can be observed in m.e.w. at 2.8 GPa, indicating that the medium penetration continues to higher pressure with respect to e.gl. system. The compressibility of HS-MOR in m.e.w. can be compared to that of the synthetic Na-MOR studied by Gatta and Lee[54] using the same PTM. HS-MOR has a lower compressibility up to about 2.8 GPa (ΔV_{HS-MOR}=-2.40% and ΔV_{Na-MOR}=-4.60%) and, in contrast, is more compressible at higher P (ΔV_{HS-MOR}=-5.48% and ΔV_{Na-MOR}=-4.83% in the 2.8-5.5 GPa range). As reported by the authors, in Na-MOR no evidence of over-hydration was suggested by the evolution of the cell-parameters, even though the lack of structural refinements prevented unambiguous descriptions of the P-induced phenomena at the atomic level. Instead, the penetration of additional guest species is the driving force in the low P regime of HS-MOR and so the structure is more rigid than that of Na-MOR. Above 3 GPa the P-V curves of HS-MOR and Na-MOR become almost parallel, suggesting similar compression mechanisms and hindrance of the extraframework species.

Upon decompression, the features of the P_{amb} powder patterns (i.e. position, shape and intensity of the peaks) are only partially regained (Figure 6). In particular, in the case of compression in e.gl., the P_{amb} intensity ratios of HS-MOR peaks is not fully regained upon decompression. The structural refinement performed at P_{amb} after the pressure release, and the cell parameters derived from the ex-situ experiments, indicate that ethylene glycol molecules are partially retained inside the mordenite micro porosities.

When compressed with penetrating PTM, the crystallinity of HS-MOR is significantly retained and no complete amorphization occurs during the experiments, in contrast to the evident loss of crystallinity observed at HP in s.o. This further confirms that the P-induced pore intrusion stiffens the structure and enhances the stability of the zeolite, supporting the framework and preventing P-induced amorphization.

Conclusions

This study demonstrates that the HP induced intrusion of guest molecules in high silica mordenite occurs at very low pressure for all the investigated penetrating media. In particular, the structural refinement of the XRPD pattern collected at 0.1 GPa in ethylene glycol reveals the presence of 3.5 e.gl molecules per unit cell, confirming the rapid intrusion of the medium in the very first stage of the compression. A fraction of these e.gl. molecules is partially retained inside HS-MOR upon pressure release, which is interesting for potential applications of this composite material.

Comparing the P-induced volume contractions observed in aqueous and non-aqueous media, we conclude that a higher amount of guest molecules is intruded in HS-MOR cavities when it is compressed in aqueous media. This is probably due to the lower dimensions of water/alcohol with respect to ethylene glycol molecules. The peak intensities of the P_{amb} patterns are never fully

regained upon P release for all the penetrating media, suggesting a partial irreversibility of the intrusion phenomena.

The Rietveld refinements of the powder patterns collected in the non-penetrating silicone oil at 0.2 and 0.8 GPa indicated that the 12MRs and 8MRs windows of MOR channels, running along the *c* axis, become more compressed along their original shorter O-O diameters. This increase in ellipticity is accompanied by a narrowing of these apertures. A symmetry lowering was observed in s.o. above 0.8 GPa, while above 1.6 GPa the patterns indicated a rapid loss of long range order.

Among the high-silica zeolites compressed in the P_{amb}-1.2 GPa range with the non-penetrating silicone oil, HS-MOR shows the highest volume contraction (6.40%). In fact, in the same *P* range, the volume variation is about 5% for silicalite-1 F and silicalite-1 OH[9], 2.6% for siliceous Y[69], and 3.96% for Si-ferrierite.[68] Since MOR has a 'framework density' (FD [47]) much higher than zeolite Y (17.2 and 12.7, respectively), these results confirm once again that zeolite compressibility is not simply related to the material porosity.

Acknowledgements

References

1 G.D. Gatta, *Z. Kristallogr.* 2008, **223**, 160-170.

2 R. Arletti, O. Ferro, S. Quartieri, A. Sani, G. Tabacchi, G. Vezzalini, *Am. Min.* 2003, 88, 1416-1422.

3 S. Ori, S. Quartieri, G. Vezzalini, V. Dmitriev, *Am. Mineral.* 2008, **93**, 1393–1403.

4 E. Fois, A. Gamba, C. Medici, G. Tabacchi, S. Quartieri, E. Mazzucato, R. Arletti, G. Vezzalini, V. Dmitriev, *Micropor. Mesopor. Mat.* 2008*, **115**, 267-280.

5 C. Betti, E. Fois, E. E. Mazzucato E., C. Medici, S. Quartieri, G. Tabacchi, G. Vezzalini, V. Dmitriev, *Micropor. Mesopor. Mat.* 2007, **103**, 190–209.

6 R. Arletti, S. Quartieri, G. Vezzalini, *Am. Min.* 2010, **95**, 1247-1256.

7 R. Arletti, G. Vezzalini, A. Morsli, F. Di Renzo, V. Dmitriev, S. Quartieri, *Micropor. Mesopor. Mat.* 2011, **142**, 696-707

8 S. Quartieri, G. Montagna, R. Arletti, G. Vezzalini, *J. Solid State Chem.* 2011, **181**, 1505-1516.

9 S. Quartieri, R. Arletti, G. Vezzalini, F. Di Renzo, V. Dmitriev, *J. Solid State Chem*. 2012, **191**, 201-212

10 L. Leardini, S. Quartieri, A. Martucci, G. Vezzalini, V. Dmitriev, *Z. Kristallogr.* 2012, **227**, 514–521.

11 L. Leardini, S. Quartieri, G. Vezzalini, A. Martucci, V. Dmitriev, *Micropor. Mesopor. Mat.* 2013, **170**, 52–61.

12 Leardini, L.; Quartieri, S.; Vezzalini, G. Compressibility of microporous materials with CHA topology: 1. Natural chabazite and SAPO-34. *Micropor. Mesopor. Mat.* 2010, **127**, 219–227.

13 G.D. Gatta. *Eur. J. Mineral.* 2005, **17**, 411-421.

14 Y. Lee, J.A. Hriljac, A. Studer, T. Vogt, *Phys. Chem. Miner.* 2004, **31**, 22–27.

15 G. Vezzalini, R. Arletti, S. Quartieri,. *Acta Cryst. B* 2014, **70**, 444–451.

16 J. Stelzer, M. Paulus, M. Hunger, J. Weitkamp, *Micropor. Mesopor. Mat.* 1998, **22**, 1-3.

17 R.N. Eissmann, M.D. LeVan, *Ind. Eng. Chem. Res*. 1993, **32**, 2752-2757.

18 N. Desbiens, I. Demachy, A.H. Fuchs, H. Kirsch-Rodeschini, M. Soulard, J. Patarin, *Angew. Chem. Int. Ed.* 2005, **44**, 5310 –5313.

19 F. Cailliez, M. Trzpit, M. Soulard, I. Demachy, A. Boutin, J. Patarin, A.H. Fuchs, *Phys. Chem. Chem. Phys.* 2008, 10, 4817–4826.

20 Y.G. Bushuev, G. Sastre, G.; J.V de Julian-Ortiz, J. Galvez, *J Phys. Chem. C* 2012, **116**, 24916 –24929.

21 M. Trzpit, S. Rigolet, J-L Paillaud, C. Marichal, M. Soulard, J. Patarin, *J. Phys. Chem. B* 2008, **112**, 7257–7266.

22 M.A. Saada, M. Soulard, B. Marler, H. Gies, J. Patarin, *J. Phys. Chem. C* 2011, **115**, 425–430.

23 M.A. Saada, S. Rigolet, J-L Paillaud, N. Bats, M. Soulard, J. Patarin, *J. Phys. Chem. C* 2010, **114**, 11650–11658.

24 D. Scelta, M. Ceppatelli, M. Santoro, R. Bini, F.A. Gorelli, A. Perucchi, M. Mezouar, A. Van der Lee, J. Haines, *Chem. Mater.* 2014, **26**, 2249–2255.

25 M. Santoro, F.A. Gorelli, R. Bini, J. Haines, A. van der Lee, *Nat. Commun.* 2013, **4**, 1557-1563.

26 E.A Havenga, Y. Huang, R.A. Secco, *Mater. Res. Bull.* 2003, **38**, 381–387.

27 Y. Huang, *Mater. Chem.* 1998, **8**, 1067–1071.

28 Y. Huang, E.A. Havenga, *Chem. Phys. Lett.* 2001, **345**, 65–71.

29 H. Lui, R.A. Secco, Y. Huang, *Phys. Chem. Commun*. 2001, **8**, 1–3.

30 P. Richet, P. Gillet, *Eur. J. Mineral.* 1997, **9**, 907–933.

31 M.D. Rutter, R.A. Secco, Y. Huang, *Chem. Phys. Lett.* 2000, **331**, 189–195.

32 M.D. Rutter, T. Uchida, R.A. Secco, Y. Huang, Y. Wang, *J.Phys. Chem. Solids* 2001, **62**, 599–606.

33 R.A. Secco, Y. Huang, *J. Phys. Chem. Solids* 1999, **60**, 999–1002.

34 S. M. Sharma, S.K. Sikka, *Prog. Mater. Sci.* 1996, **40**, 1–77.

35 J. Gulin-Gonzalez, G.B. Suffritti, *Micropor. Mesopor. Mat*. 2004, **69**,127–134.

36 E. Fois, A. Gamba, G. Tabacchi, R. Arletti, S. Quartieri, G. Vezzalini, *Am. Mineral.* 2005, **90**, 28-35.

37 E. Fois, A. Gamba, G. Tabacchi, S. Quartieri, R. Arletti, G. Vezzalini, *Stud. Surf. Sci. Catal.* 2005, **155**, 271-280.

38 I. Peral, J. Iniguez, *Phys. Rev. Lett.* 2006, **97**, 225502/1-4.

39 D. W. Breck, Zeolite molecular sieves; Wiley: New York, 1974.

40 W. M.Meier, J. B. Uytterhoeven, Molecular Sieves; Adv. Chem. Ser.: Washington DC, American Chemical Society, 1973.

41 A. Martucci, L. Pasti, M. Nassi, A. Alberti, R. Arletti, R. Bagatin, R. Vignola, R. Sticca, *Micropor. Mesopor. Mat.* 2012, **151**, 358-367.

42 A. Martucci, L. Pasti, N. Marchetti, A. Cavazzini, F. Dondi, A. Alberti, *Micropor. Mesopor. Mat.* 2012 **148**, 174–183.

43 R. Arletti, A. Martucci, A. Alberti, L. Pasti, M. Nassi, R. Bagatin, *J. Solid State Chem*. 2012, **194**, 135-142.

44 A. Martucci, M.A., Cremonini, S. Blasioli, L. Gigli, G. Gatti, L. Marchese, I. Braschi, *Micropor. Mesopor. Mat.* 2013, **170**, 274–286.

45 V. Sacchetto, G. Gatti, G. Paul, I. Braschi, G. Berlier, M. Cossi, L. Marchese, R. Bagatin, C. Bisio, *Phys. Chem. Chem. Phys.* 2013, **15**, 13275-13287.

46 S. Blasioli, A. Martucci, G. Paul, L. Gigli, M. Cossi, C.T. Johnston, L. Marchese, I. Braschi, *J. Colloid Interface Sci.* 2014, **419**, 148-159.

47 C.H. Baerlocher, L.B. McCusker, D.H. Olson, *Atlas of Zeolite Framework Types sixth revised*; Elsevier: Amsterdam, 2007.

48 G. Gottardi, E. Galli, *Natural zeolites*; Springer-Verlag: Berlin, 1985, p. 409.

49 E. Passaglia, R.A. Sheppard, In *Natural zeolites: occurrence, properties, application. Reviews in mineralogy and geochemistry*; Bish, D.L., Ming D.W., Eds.; Mineralogical Society of America and Geochemical Society: Washington DC, 2001; pgs. 69–116.

50 R.M. Barrer, E.A.D. White, *J. Chem. Soc.* 1952, 1561-1571.

51 W.M. Meier, *Z. Kristallogr.* 1961, **115**, 439–450.

52 A. Martucci, M. Sacerdoti, G. Cruciani, C. Dalconi, *Eur. J. Mineral.* 2003, **15**, 485–493.

53 G.D. Gatta, Y. Lee, *Phys. Chem. Minerals* 2006, **32**, 726–732.

54 G.D. Gatta, Y. Lee, *Mineral. Mag*. 2014, **78**, 267–291.

55 P. Lotti, G.D. Gatta, M. Merlini, , H-P Liermann, *Z. Kristallogr.* doi 10.1515/zkri-2014-1796, in press.

56 A.P. Hammersley, S.O. Svensson, M. Hanfland, A.N. Fitch, D. Häusermann, *High Pressure Res.* 1996, **14**, 235–248.

57 A.C. Larson, R.B. Von Dreele*, General Structure Analysis System "GSAS";* Los Alamos National Laboratory Report; Los Alamos, 1994; LAUR 86-748.

58 B.H. J. Toby, *Appl. Crystallogr.* 2001, **34**, 210–213

59 P. Thompson, D.E. Cox, J.B. Hastings, *J. Appl. Crystallogr.* 1987, 79–83.

60 R. Miletich, D.R. Allan, W.F. Kush, In *High-Temperature and High-Pressure Crystal Chemistry, Reviews in Mineralogy and Geochemistry, vol. 41,* Hazen, R.M., Downs, R.T., Eds.; Mineralogical Society of America and Geochemical Society: Washington, USA, 2000; vol. 41,pp 445–519

61 R.A. Forman, G.J. Piermarini, J.D.Barnett, S. Block, *Science* 1972 **176**, 4673–4676.

62 H.K. Mao, J. Xu, P.M. Bell, *J. Geophys. Res*. 1986, **91**, 4673–4676.

63 C. Murli, N. Lu, Z. Dong, Y. Song, *J. Phys. Chem. B* 2012, **116**, 12574–12580.

64 M. Santoro, F. Gorelli, J. Haines, O. Cambon, C. Levelut, G. Garbarino, *Proc. Natl. Acad. Sci. U. S. A.* 2011, **108**, 7689-7692.

65 B. Coasne, J. Haines, C. Levelut, O. Cambon, M. Santoro, F. Gorelli, G. Garbarino, *Phys. Chem. Chem. Phys.* 2011, **13**, 20096-20099.

66 A. Sartbaeva, J. Haines, O. Cambon, M. Santoro, F. Gorelli, C. Levelut, G. Garbarino, S.A. Wells, *Phys. Rev. B* 2012, **85**, 064109/1-5

67 J. Haines, O. Cambon, C. Levelut, , M. Santoro, F. Gorelli, G. Garbarino, *J. Am. Chem. Soc.,* 2010, **132**, 8860-8861.

68 R. Arletti, G. Vezzalini, S. Quartieri, F. Di Renzo, V. Dmitriev, *Micropor. Mesopor. Mat*. 2014, **191**, 27–37.

69 M. Colligan, P.M. Forster, A.K. Cheetham, Y. Lee, T. Vogt, J.A. Hriljac, *J. Am. Chem. Soc.* 2004,**126**, 12015-12022.

70 J. Haines, C. Levelut, A. Isambert, P. Hebert, S. Kohara, D.A. Keen, T. Hammouda, D. Andrault, *J. Am. Chem. Soc.* 2009, **131**, 12333–12338.